

# Optron: Better Medical Image Registration via Optimizing in the Loop

Yicheng Chen <sup>\*</sup>  
 Tongji University  
 Shanghai, China  
 2053186@tongji.edu.cn

Yuelin Xin <sup>\*</sup>  
 University of Leeds  
 Leeds, UK  
 sc20yx2@leeds.ac.uk

Kun Han  
 University of California, Irvine  
 Irvine, CA, USA  
 khan7@uci.edu

Shengxiang Ji <sup>\*</sup>  
 Huazhong University of Science and Technology  
 Wuhan, China  
 u202015362@hust.edu.cn

Xiaohui Xie  
 University of California, Irvine  
 Irvine, CA, USA  
 xhx@ics.uci.edu

## Abstract

Previously, in the field of image registration, there are mainly two paradigms, the traditional optimization-based methods, and the deep-learning-based methods. In this work, we aim to combine the advantages of both paradigms. We designed a robust training architecture that is simple and generalizable. We present **Optron**, a general training architecture incorporating the idea of optimizing-in-the-loop. By iteratively optimizing the prediction result of a deep learning model through a plug-and-play optimizer module in the training loop, Optron introduces pseudo ground truth to an unsupervised training process. This pseudo supervision provides more direct guidance towards model training compared with unsupervised methods. Utilizing this advantage, Optron can consistently improve the models' performance and convergence speed. We evaluated our method on various combinations of models and datasets, and we have achieved state-of-the-art performance on the IXI dataset, improving the previous state-of-the-art method TransMorph by a significant margin of +1.6% DSC. Moreover, Optron also consistently achieved positive results with other models and datasets. It increases the validation DSC on IXI for VoxelMorph and ViT-V-Net by +2.3% and +2.2% respectively, demonstrating our method's generalizability. Our implementation is publicly available at <https://github.com/miraclefactory/optron>

## 1. Introduction

Medical image registration is critical in many aspects of medical image analysis and has numerous applications in

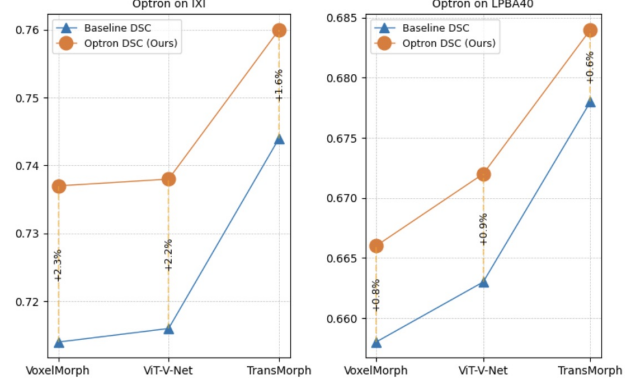


Figure 1. We benchmarked Optron with various deep learning models (VoxelMorph [7], ViT-V-Net [12], TransMorph [11]) and datasets (showing IXI [24] and LPBA40 [38] here). We observed significant and consistent improvement over the purely deep-learning-based methods on Dice score. We have achieved +1.6% higher DSC on IXI compared with the previous state-of-the-art method TransMorph [11].

modern medicine. At its core, it is a problem of finding transformations (i.e., a deformation field) to fit two medical images (such as volumetric MRIs) together in such a way that they look as similar as possible. Two types of methods are commonly used to address this problem, optimization-based methods and deep-learning-based methods.

Traditionally, optimization-based methods like [4, 6, 31], are used to iteratively improve the deformation field, enabling the pair of images to fit better together. More recently, with the emergence and dominance of deep learning methods, the field of image registration has also adopted these types of methods which predict deformation fields directly from the fixed and moving images. These two types of methods have been producing impressive results, how-

<sup>\*</sup>Equal contribution

ever, since the emergence of models using Transformer-based [15] backbone networks [11, 12], the deep learning approach has gradually surpassed traditional methods as the new bar of image registration tasks. Nonetheless, traditional optimization-based methods still have their merits. While these optimization-based methods tend to be more computationally intensive, they are more stable and can produce smoother deformation fields. Furthermore, using the idea of this optimization-based approach, we can potentially build a more direct heuristic to guide the training of deep learning models compared with unsupervised training.

In this paper, we will present and explore a novel training architecture, called ***Optron***, which utilizes optimized deformation fields as pseudo ground truth to provide pseudo supervision for deep networks during the training process. In our method, the training architecture will be divided into two stages, the prediction stage and the optimization stage. Firstly, a deep network is used to predict a deformation field during the forward pass, then, this predicted deformation field will be used as the initialization parameters of the optimizer module. The optimizer module will then iteratively refine its parameters (the deformation field) and produce an optimized deformation field. The optimized field will be used as pseudo ground truth to supervise the deep network. This pseudo supervision is derived by calculating the mean square error loss between the optimized deformation field and the one predicted by the deep learning network. This heuristic will be used to guide the unsupervised training process and make it pseudo-supervised. By bringing the training process closer to that of supervised training, we can improve the model’s performance and increase its convergence speed.

We benchmarked our method using various deep learning models and datasets. Optron showed a consistent advantage over the original deep-learning-based methods. In order to demonstrate the architecture’s robustness and generalizability, we didn’t introduce any model-specific adjustment or hyperparameter settings. On the previous state-of-the-art model TransMorph [11], we were able to improve its performance by +1.6% on DSC on the IXI dataset [24] by training it with the Optron architecture. We have also observed a significant decrease in Jacobian determinant which suggests the model now predicts smoother deformation fields with less spatial folding and topological anomalies.

The main contributions of our work are summarized as follows:

- We present the Optron training architecture, an effective, generalizable, plug-and-play method to improve the training outcome of deep learning registration models.
- We incorporated the idea of optimizing-in-the-loop

to build a close collaboration between deep learning models and the optimizer module within the training loop. Using pseudo supervision provided by the optimizer module, we can train the models to a higher capacity compared with unsupervised training.

- We benchmarked our method with various models and datasets, and we have achieved better performance compared with the previous state-of-the-art method TransMorph [11] on the IXI dataset [24], along with consistent performance increase with other models tested.

## 2. Related Work

Deformable image registration computes a dense correspondence between two images, typically involving two steps: an initial affine transformation for global alignment, and a subsequent deformable transformation with a higher degree of freedom. In this work, our primary focus is on the latter step.

### 2.1. Traditional Registration Methods

Traditional registration methods solve an optimization problem in the space of deformation fields with certain model assumptions. They iteratively minimize a custom energy function Eq. (5) for each pair of images [1].

These traditional methods include elastic-type methods [6, 31], free-form deformations with b-splines [23], statistical parametric mapping [2], discrete methods [3, 17], and Demons [37]. Additionally, some diffeomorphic methods have demonstrated comparable or even superior results, such as Large Diffeomorphic Distance Metric Mapping (LDDMM) [8, 16] and symmetric normalization (SyN) [4].

Our proposed Optron optimizer module utilizes the merits of traditional methods by iteratively optimizing each pair of images, while implicitly maintaining smooth and topology-preservation transformations through regularization, rather than relying on strong model assumptions.

### 2.2. Deep-Learning-based Registration Methods

The learning-based registration algorithms [7, 13, 18, 26–30, 32–35, 39] optimize the energy function in Eq. (5) for training dataset, and acquire a global representation of the images being registered. As a result, they can predict deformation vector fields (DVF) for unseen data. Based on the different backbone architecture, previous learning-based methods are categorized into two main types: ConvNet-based methods and Transformer-based methods.

**ConvNet-based methods.** Some ConvNet-based approaches require the supervision of ground truth deformation fields. These ground truths are typically gener-

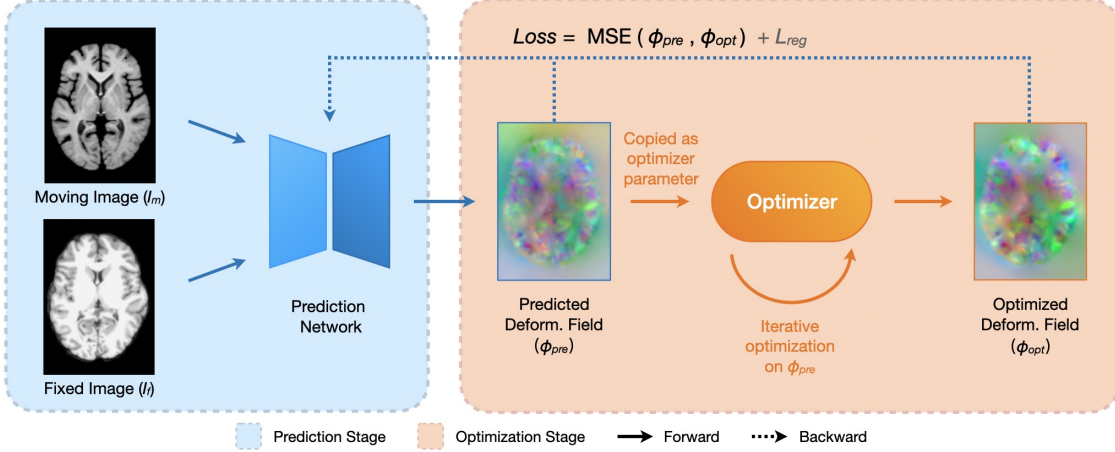


Figure 2. The overall structure of the proposed Optron architecture. The whole architecture is divided into two parts, the prediction stage (any network that can produce a deformation field given a pair of images), and the optimization stage. Optron uses the idea of optimizing-in-the-loop to integrate the optimizer into the training process of the prediction network. The optimizer will iteratively refine the deformation field produced by the prediction network, the derived optimized deformation field will then be used as pseudo ground truth to train the prediction network. As this graph illustrates, a loop is formed between the prediction network and the optimizer module. Detailed internal structure of the optimizer module is in Figure 3.

ated by traditional registration methods or manual annotation. Quicksilver [39] is a supervised deep encoder-decoder network that generates the momentum-parameterization of LDDMM [8] from image patches. RegNet [35] is trained by artificially generated deformation fields. Several methods explore unsupervised strategies with the key innovation, spatial transformer network (STN) [20]. VoxelMorph [7] utilizes U-Net to predict the deformation field. Bob D. de Vos et al. [14] proposed a framework for affine and deformable image registration, offering a method for coarse-to-fine image registration. Zhengyang Shen et al. [32] proposed a deep-learning framework for diffeomorphic transformations through a vSVF model. However, these ConvNet-based methods above are usually limited in learning global and long-range dependent information.

**Transformer-based methods.** In recent developments, Transformer-based architectures have been applied in many computer vision tasks, such as image recognition [15], object detection [9], and segmentation [36]. In medical image registration, transformer-based methods solve the limitations of ConvNets and achieve state-of-the-art performance. DTN [40] uses a transformer block over the CNN backbone to capture semantic contextual relevance. ViT-V-Net [12] is the first to apply Vision Transformer [15] in volumetric image registration, which embeds a ViT block at the bottleneck of a U-Net architecture [19] to learn long-distance relationships between high-level features of the moving and fixed images. TransMorph [11] is a new hybrid Transformer-ConvNet model, which uses Swin Transformer [22] as the encoder and ConvNet as the decoder.

### 3. Method

In this work, we present a novel, robust, two-stage training architecture called Optron, utilizing the idea of optimizing-in-the-loop. It demonstrated consistent improvement across various deep learning models and datasets for medical image registration tasks. In the following sections, we will discuss the overall architecture of Optron, the design of the optimizer module, alongside the implementation details of the architecture.

In the following discussion,  $I_m$  and  $I_f$  denote the moving image and fixed image respectively and  $\phi$  denotes the deformation field.

#### 3.1. Optron Architecture

Figure 2 presents the overall structure of the proposed Optron architecture. There are two stages in our method.

**Prediction stage.** This stage consists of a prediction model. The prediction model takes in the fixed image  $I_f$  and the moving image  $I_m$ , and constructs a nonlinear transformation function  $F$  through its deep network which generates a dense deformation field  $\phi$  for each image pair  $I_f$  and  $I_m$ , i.e.,

$$F_\theta(I_f, I_m) = \phi \quad (1)$$

where  $\theta$  denotes the parameters of the deep neural network. Since the prediction stage can be any deformable registration model that predicts a deformation field, we used several popular models, such as VoxelMorph [7], ViT-V-Net [12] and TransMorph [11] as our prediction model in our experiments. It is the nature of our method that the Optron architecture could in theory work with any of such models, and

it is a plug-and-play method that can be easily applied. This generalizability will be further examined in later sections.

**Optimization stage.** The optimization stage uses an optimizer module that iteratively optimizes the initial deformation field  $\phi_{pre}$  predicted by the first stage. Subsequently, the optimized deformation field  $\phi_{opt}$  is used as the pseudo ground truth to provide supervision for the prediction model during training time, forming a loop between the prediction model and the optimizer module. More details about the internal implementation of the optimizer module can be found in Sec. 3.2.

Our method, Optron, establishes a strong collaboration between learning-based methods (prediction stage) and iterative optimization-based methods (optimization stage). Within a training loop, both methods are used together to form a bootstrapping relation, which is proven to be critical at the beginning of the training process in our experiments later. During inference time, we exclude the optimizer module and only use the prediction model itself to generate deformation fields, enabling time-efficient registration. Using this architecture will provide several crucial benefits, most notably the two below.

**Computational Efficiency.** In contrast to traditional registration methods, in which optimization is typically very slow without a good initialization, the optimization process in our training loop is much faster since we have a good initialization from the prediction model. With a reasonable initial estimate, the iterative optimization process can be accelerated dramatically, enabling us to achieve comparable optimization results with fewer iterations. In other words, this initialization, often approaching the actual optimal solution, enables the optimizer to bypass extensive search over the parameter space to a large extent. Moreover, a limited number of iterations makes this approach more practical within the training loop.

**Self-improving.** The two stages in the proposed architecture form a bootstrapping relation, and such architecture is self-improving by nature. A well-estimated deformation field from the prediction model can lead to a better-optimized deformation field. Likewise, a better deformation field from iterative optimization offers better pseudo supervision to the prediction model. This underscores the significance of optimizing-in-the-loop since it enables a tight collaboration between these two components.

### 3.2. Optimizer Module

An efficient and effective optimizer module is the key for optimizing-in-the-loop. We explored three different optimization strategies: cascaded and downsample approaches, and the proposed optimizer as shown in Figure 3. Below we provide the details on these strategies.

**Cascaded Optimizer.** One possible approach is to use a recursive cascaded network that sequentially warps the

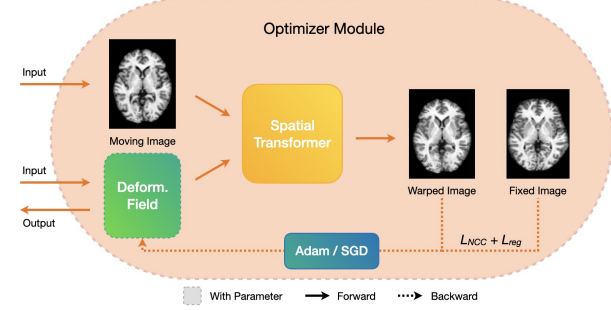


Figure 3. A diagram of the internal structure of the proposed optimizer in Optron. The optimizer takes in the moving image and an initial deformation field predicted by a deep learning model, and it outputs the optimized deformation field.

moving image [41]. Instead of predicting a final deformation field straightforwardly, this approach predicts a small displacement at each cascade that can be refined by deeper recursions. Intuitively, this optimization process is similar to the idea of residuals. During an optimization iteration, the warped image generated by the prediction model initializes the optimizer module. The pseudo ground truth, essential for the prediction model, is derived through the fusion of the generated deformation field sequence.

**Optron Optimizer.** The basic structure of the proposed Optron optimizer module is illustrated in Figure 3. The optimizer takes in the deformation field generated by the prediction model as learnable parameters. Internally, it contains a single Spatial Transformer Network (STN) [20] layer, which introduces no additional parameter. Consequently, the only learnable parameters in the optimizer is the deformation field. During an optimization iteration, the deformation field is applied to the moving image through the Spatial Transformer, yielding a warped image. Then, a image similarity loss between this warped image and the fixed image is calculated. The loss is backpropagated using methods like Adam [21] or Stochastic Gradient Descent (SGD), this essentially updates the deformation field.

**Downsample Optimizer.** By downsampling the deformation field, we can potentially decrease the number of parameters being updated in every optimization iteration, which could lead to faster optimization routines. Additionally, downsampled deformation field can provide coarse-resolution information [26], which is crucial to the smoothness of the deformation field. But our experiments showed that this method was ineffective and failed to optimize the deformation field adequately. We will compare and analyze the result in Sec. 4.6.2.

The reason of using the Optron Optimizer over the other ones can be summarized as follows:

- In order to prove the usefulness of the Optron archi-

ture, we do not need a complex optimizer. In fact, a simple one is more desirable for its structural simplicity ensures minimal effect on the validation of our proposed architecture.

- Optimizing a unique deformation field for different pairs of images instead of using a shared set of parameters can provide more image-specific heuristics and thus benefit more when used as pseudo ground truth.
- Optimizing the deformation field directly provides higher degrees of freedom with parameter adjustment, facilitating the production of better pseudo ground truth.

In the ablation study later on, we empirically demonstrated that our optimizer design achieves the highest registration accuracy compared to other approaches.

### 3.3. Implementation Detail

**Overall Loss.** Let  $\phi_{pre}$ ,  $\phi_{opt}$  denote the predicted deformation field and the optimized deformation field respectively. Given these two values, we can train our prediction model with loss supplied by pseudo supervision:

$$L_{opt} = \|\phi_{pre} - \phi_{opt}\| \quad (2)$$

In our design, we used MSE for  $L_{opt}$ .

The overall loss function  $L_{all}$  for the prediction model training consists of two parts:  $L_{opt}$  that penalizes the difference between  $\phi_{pre}$  and  $\phi_{opt}$ , and  $L_{reg}$  that provides regularization for the predicted deformation field  $\phi_{pre}$ :

$$L_{all} = L_{opt} + \lambda L_{reg} \quad (3)$$

where  $\lambda$  is the weight of the regularization loss.  $\lambda$  is preferably set to 0.02.  $L_{reg}$  acts as a diffusion regularizer on the spatial gradients of deformation field  $\phi$ :

$$L_{reg}(\phi) = \sum_{p \in \Omega} \|\nabla \phi(p)\|^2 \quad (4)$$

where  $\Omega$  represents the 3-dimensional space.

**Optimizer Module Loss.** The objective function to be minimized in the optimizer module consists of two components: an image similarity loss term that computes the difference between the warped image  $I_m \circ \phi$  and fixed image  $I_f$  and a regularization loss term that imposes smoothness in  $\phi$ :

$$L(I_m, I_f, \phi) = L_{sim}(I_m \circ \phi, I_f) + L_{reg}(\phi) \quad (5)$$

where  $\circ$  represents the transformation function which warps  $I_m$  to  $I_f$  using  $\phi$ .

The regularization term we used is the same as Eq. (4) and the similarity metric we used is the local normalized

cross-correlation (NCC) between warped image  $I_m \circ \phi$  and fixed image  $I_f$ :

$$LNCC(I_f, I_m \circ \phi) = \sum_{p \in \Omega} \frac{(\sum_{p_i} (f(p_i) - \hat{f}(p))([I_m \circ \phi](p_i) - [\hat{I}_m \circ \phi](p)))^2}{(\sum_{p_i} (f(p_i) - \hat{f}(p))^2)(\sum_{p_i} ([I_m \circ \phi](p_i) - [\hat{I}_m \circ \phi](p))^2)} \quad (6)$$

where  $\hat{I}_f(p)$  and  $\hat{I}_m(p)$  represent the mean voxel value within a local window of size  $n^3$  centered at voxel  $p$ .

## 4. Experiments

### 4.1. Datasets and Preprocessing

Here, we provide a concise overview of datasets we used for both training and evaluation. Our reported results are mainly based on three publicly available datasets of 3D brain MRI scans: the Information eXtraction from Images (IXI) dataset [24], the OASIS dataset [25] and LONI Probabilistic Brain Atlas 40 (LPBA40) dataset [38]. FreeSurfer [5] was used to perform standard preprocessing procedures on structural brain MRI data for all datasets. These procedures include skull stripping, resampling, and affine transformation. Detailed descriptions of each dataset can be found below.

**IXI dataset.** In the context of atlas-to-patient brain MRI registration, we used the preprocessed IXI dataset provided by [11]. This dataset contains a total of 576 T1-weighted brain MRI volumes and each volume has a resolution of  $160 \times 192 \times 224$ . We randomly selected 200 volumes for training and 20 volumes for validation. 30 anatomical structures in segmentation maps were used to evaluate registration performance.

**OASIS dataset.** For inter-patient registration task, we used the preprocessed OASIS dataset provided by [11]. This dataset consists a total of 451 brain T1 MRI volumes with size  $160 \times 192 \times 224$ . We randomly selected 200, 19 volumes for training and validation respectively. 35 anatomical structures in segmentation maps were used to evaluate registration performance.

**LPBA40 dataset.** We additionally used the LPBA40 dataset [38] to validate our method. It includes 40 patients with brain MRI volumes and ground truth segmentation masks. Each volume has a resolution of  $160 \times 192 \times 160$ . We used 30 volumes for training, 9 volumes for validation, and 1 volume as atlas. 54 anatomical structures in segmentation maps were used to evaluate registration performance.

### 4.2. Evaluation Metrics

We used Dice Similarity Coefficient (DSC), Jacobian Determinant and Registration Speed to evaluate the performances of our trained registration models. DSC measures the volume overlap between anatomical segmentations of the fixed image and warped moving image. Negative Ja-

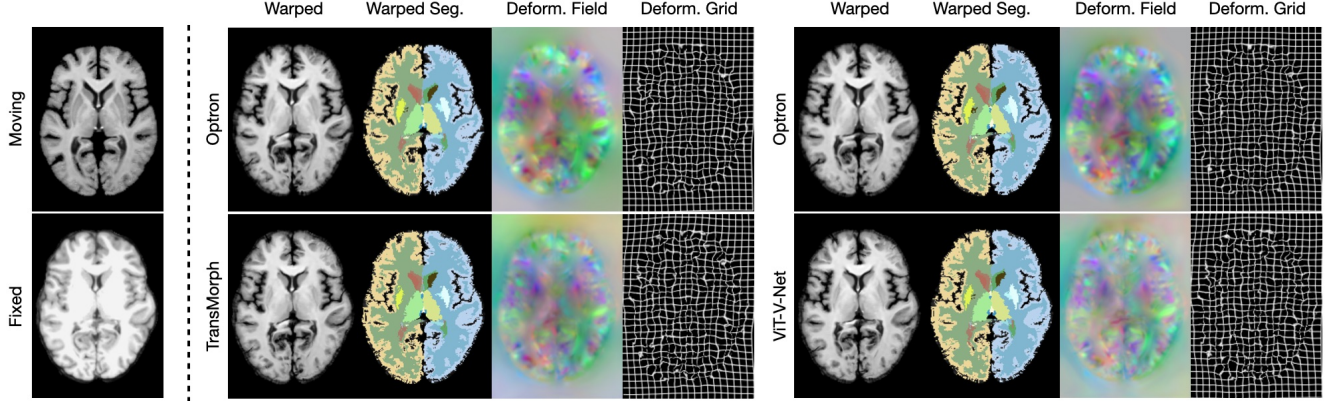


Figure 4. Visualization of registration results. This is an arbitrary demo extracted from the comparison results between baseline TransMorph, ViT-V-Net (row 2) and their respective model trained with Optron (row 1), demo from the IXI dataset [24]

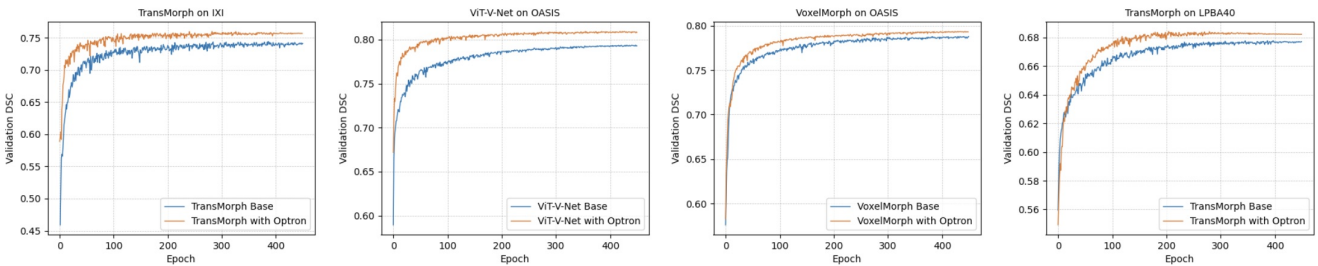


Figure 5. Demo visualization of training process vs. validation DSC for some combinations of models and datasets. Showing significant improvements over the original models. Optron provides crucial guidance for model training during the early stage of the training process.

cobian Determinant captures local distortion in the neighborhood. We quantify the regularity of the deformation fields using the percentage of non-positive values in the determinant of the Jacobian matrix on the deformation fields ( $\%|J_\phi| < 0$ ). A lower percentage of negative Jacobian determinant indicates a smoother deformation field. We additionally computed the average time of registration for each image pair to evaluate the registration speed.

### 4.3. Experiment Settings

All models were trained on an NVIDIA RTX 4090 GPU for 500 epochs using the Adam optimization algorithm, with an initial learning rate of 1e-4 and a batch size of 1. The dataset was augmented with flipping in random directions during training. For the optimizer module in our architecture, we used an initial learning rate of 0.1 and an optimization iteration number of 10 during training.

### 4.4. Baseline Methods

We validated our proposed architecture based on various registration methods that have previously demonstrated state-of-the-art performance in registration tasks. We compared our method to two traditional methods. Detailed hy-

perparameter settings for each method are as follows:

- SyN [4]: For all datasets, mean squared error (MSE) was used as the objective function, along with three scales with 160, 80, 40 iterations, respectively.
- NiftyReg [10]: The sum of squared difference (SSD) was used as the objective function. We used three scales with 300 iterations each by default.

We also compared our method with several state-of-the-art deep-learning-based methods. For a fair comparison and more reliable results, we used LNCC (Eq. (6)) and a regularizer (Eq. (4)) as the loss function (Eq. (3)) for all models. The regularization weight  $\lambda$  was set to 1 as suggested in [7]. Note that we didn't use Dice loss, since we want to establish our baselines on fully unsupervised training. Hyperparameter settings for each method are as follows:

- VoxelMorph [7]: This registration network was based on U-net [19]. We used the default parameters of VoxelMorph-1 proposed in [7].
- ViT-V-Net [12]: This registration network was developed based on ViT [15]. We applied the default network hyperparameter settings suggested in [12].

Datasets	Methods	Base. DSC	<b>Optron DSC</b>	Base. $ J_\phi  < 0$ (%)	<b>Optron</b> $ J_\phi  < 0$ (%)	Inference Time (s)
IXI [24]	SyN [4]	0.647	N/A	1.96e-6	N/A	277(CPU)
	NiftyReg [10]	0.585	N/A	0.029	N/A	22.4(CPU)
	VoxelMorph [7]	0.714	<b>0.737</b>	1.398	<b>0.516</b>	0.061(GPU)
	ViT-V-Net [12]	0.716	<b>0.738</b>	1.543	<b>0.545</b>	0.615(GPU)
OASIS [25]	TransMorph [11]	0.744	<b>0.760</b>	1.433	<b>0.794</b>	0.114(GPU)
	SyN [4]	0.769	N/A	1.58e-4	N/A	258(CPU)
	NiftyReg [10]	0.762	N/A	0.011	N/A	25.0(CPU)
	VoxelMorph [7]	0.788	<b>0.794</b>	0.911	<b>0.490</b>	0.061(GPU)
LPBA40 [38]	ViT-V-Net [12]	0.794	<b>0.809</b>	0.887	<b>0.487</b>	0.646(GPU)
	TransMorph [11]	0.818	<b>0.818</b>	0.765	<b>0.517</b>	0.160(GPU)
	SyN [4]	0.703	N/A	1.18e-4	N/A	172(CPU)
	NiftyReg [10]	0.691	N/A	1.13e-3	N/A	22.8(CPU)
LPBA40 [38]	VoxelMorph [7]	0.658	<b>0.666</b>	0.288	<b>0.023</b>	0.046(GPU)
	ViT-V-Net [12]	0.663	<b>0.672</b>	0.390	<b>0.112</b>	0.446(GPU)
	TransMorph [11]	0.678	<b>0.684</b>	0.438	<b>0.150</b>	0.327(GPU)

Table 1. Evaluation results for different methods on various datasets. The Optron architecture provides significant improvement on the purely deep learning methods. All inference time measured on CPU is tested on a 8-core Intel Xeon CPU (Skylake), all inference time measured on GPU is tested on an NVIDIA RTX 4090 GPU.

- TransMorph [11]: This registration network was developed based on Swin Transformer [22]. We applied the default hyperparameter settings of TransMorph in [11].

## 4.5. Results

### 4.5.1 Optron on IXI

We evaluated our method on the IXI dataset which is also used in TransMorph [11], so that we can make quick comparison on the enhancement of using the Optron architecture on the state-of-the-art method. Our evaluation result on the IXI dataset is shown in Tab. 1. The first image in Figure 5 visualizes the training process of TransMorph on IXI.

Notably, Optron considerably increased DSC and convergence speed over the original deep learning models. In particular, we were able to improve upon the previous state-of-the-art method TransMorph [11] on the IXI dataset by +1.6% on DSC and halving its percentage of  $|J_\phi| < 0$ . This suggests that not only can Optron improve the model’s performance, but it can also prevent the model from producing an over-sharpened deformation field, which can be visually observed by comparing the actual registration results as shown in Figure 4.

We have also improved other deep learning methods considerably, with a +2.3% increase on DSC for VoxelMorph [7] and a +2.2% increase on DSC for ViT-V-Net [12], further validating the effectiveness and generalizability of our method.

Converg. Loss	IXI [24]	OASIS [25]	LPBA40 [38]
VoxelMorph [7]	-0.222	-0.259	-0.183
ViT-V-Net [12]	-0.242	-0.266	-0.215
TransMorph [11]	-0.262	<b>-0.283</b>	-0.232

Table 2. Comparison between the 3 models’ convergence losses on 3 datasets. Note that the loss function settings were the same. For TransMorph on OASIS [25], the convergence loss is clearly the lowest.

### 4.5.2 Optron on OASIS

OASIS [25] is another commonly used dataset in medical image registration. According to the results in Tab. 1, all methods generally achieve higher DSC on this dataset.

The training process of ViT-V-Net and VoxelMorph on OASIS are visualized in the second and third image in Figure 5, which further proves that our method can significantly improve model performance and convergence speed.

We found that Optron introduced a limited improvement over TransMorph on OASIS. This can be explained as the OASIS dataset is less challenging for TransMorph which has strong fitting capability. This claim can be easily validated by comparing the convergence loss of all the models across different datasets as shown in Tab. 2. Across multiple combinations of the 3 models and 3 datasets, TransMorph on OASIS has the lowest convergence loss, which verifies our hypothesis.

$\alpha:\beta$	1:1	1:10	1:100	1:1000	0
DSC	0.427	0.407	0.453	0.489	<b>0.728</b>

Table 3. Ablation study on the impact of the ratio of  $\alpha$  (weight of  $L_{sim}$ ) to  $\beta$  (weight of  $L_{opt}$ ). The weight of  $L_{reg}$ ,  $\lambda$ , is always 0.02. In the case that the ratio of  $\alpha$  to  $\beta$  equals 0 (i.e. Eq. (3)),  $\alpha$  and  $\beta$  equal to 0 and 1 respectively. This study was conducted using TransMorph [11] with Optron on the IXI dataset [24] and we compared DSC at the 30th epoch. Note that the raw DSC after affine preprocessing is 0.407. Except the overall loss function, other experiment settings remains the same.

#### 4.5.3 Optron on LPBA40

LPBA40 [38] is another dataset we used to validate our method. Evaluation results are presented in Tab. 1. With only 40 volumes, deep learning models can easily overfit on this dataset. This can be partially observed in the 4th image in Figure 5.

On a small dataset, the extra supervision provided by our method can be crucial due to the lack of training data. A supervision that can motivate the training process by giving the model more challenge, can benefit the training process and yielding a better result.

### 4.6 Ablation Study

#### 4.6.1 Loss Composition

Since we developed our method based on widely-used unsupervised approaches that utilize image similarity metrics to train their models, our initial idea was to add  $L_{opt}$  to the unsupervised loss function  $L_{us}$  in [7] as an extra and auxiliary pseudo supervision, i.e.

$$\begin{aligned} L_{all} &= L_{us} + \beta L_{opt} \\ &= \alpha L_{sim} + \lambda L_{reg} + \beta L_{opt} \end{aligned} \quad (7)$$

We experimented with several different ratios of  $\alpha$  to  $\beta$ . From the experimental results shown in Tab. 3, we found that adding  $L_{sim}$  led to abnormal validation results, in which the model failed to converge. The reason is likely that  $L_{sim}$  and  $L_{opt}$  had very different effects on the training process. To be specific, the prediction model explores in the parameter space according to the heuristics from  $L_{sim}$ . In contrast,  $L_{opt}$  provides more accurate and direct guidance through pseudo ground truth which tend to be closer to the actual optimal solution after multiple optimization steps. Their gradient vectors may diverge into two different directions. Hence, their effects can offset each other when combined, preventing the model from converging. Thus, the term  $L_{sim}$  was not used in Eq. (7) aiming to maximize the advantage of pseudo ground truths. Experiment results demonstrate that our overall loss function(i.e. Eq. (3)) is reasonable and can obtain better registration accuracy.

Optimizers	DSC	Time (s)	VRAM Usage
None	0.635	N/A	12.07 GB
Cascaded	0.638	11.24	38.62 GB
DownSample	0.610	<b>0.097</b>	12.44 GB
Optron	<b>0.654</b>	3.228	13.07 GB

Table 4. Ablation study with different optimizer schemes on LPBA40 dataset. We evaluated their performance using the validation dataset during the first 30 epochs.

#### 4.6.2 Optimizer Design

Tab. 4 shows the performance of different optimizer schemes. The Cascade Optimizer contains two cascades within the optimizer. And each optimizer runs for 10 iterations. Notably, the initial learning rate is set at 1e-4 for the Cascade Optimizer, given its network-based nature, while it is set to 0.1 for the Downsample Optimizer and Optron Optimizer.

We can observe that all the optimizers demonstrate their effectiveness by surpassing the performance of none-optimizer version, except for the Downsample Optimizer. Among the compared strategies, the proposed Optron optimizer module achieves the highest Dice score while maintaining practical optimization time within the training loop. For the Downsample Optimizer, while it does improve optimization speed, direct downsampling of the deformation field leads to errors in coarse resolution and loss of fine-granularity information. Regarding the Cascade Optimizer, though the improvement limit is not observed with the increasing cascades [41], the computational intensity and optimization time is impractical in our proposed architecture. Additionally, one significant challenge in the development and implement of the Cascaded Optimizer is an effective method to fuse the deformation fields sequence.

## 5. Conclusion

This work introduces Optron, a general architecture using the idea of optimizing-in-the-loop. It combines learning-based methods and optimization-based methods to train a deep learning network for medical image registration tasks. Our approach uses the learning-based models to predict an initial deformation field for the optimizer module, which then refines the deformation field iteratively and provides pseudo ground truth for the training of the learning-based models.

Our proposed architecture outperforms previous approaches by large margins, and we were able to achieve state-of-the-art performance on the IXI dataset, as well as consistent improvements on other cases, proving its effectiveness and generalizability.

We hope our work has laid down a feasible architecture

for optimizing-in-the-loop registration methods, and provides a solid base for future works to build upon. In our current implementation, the training process of Optron is still more time-consuming compared with pure deep learning methods due to the extra optimization steps for each pair of images. Future work could consider improving the design and efficiency of the optimizer module which can benefit this architecture to a greater extent.

## References

- [1] Sotiras A, Davatzikos C, and Paragios N. Deformable medical image registration: a survey. *IEEE Trans Med Imaging*, 2013. [2](#)
- [2] John Ashburner and Karl J. Friston. Voxel-based morphometry—the methods. *NeuroImage*, 2000. <https://doi.org/10.1006/nimg.2000.0582>. [2](#)
- [3] Dalca AV, Bobu A, Rost NS, and Golland P. Patch-based discrete registration of clinical brain images. *Patch Based Tech Med Imaging (2016)*, 2016. [2](#)
- [4] B.B. Avants, C.L. Epstein, M. Grossman, and J.C. Gee. Symmetric diffeomorphic image registration with cross-correlation: Evaluating automated labeling of elderly and neurodegenerative brain. *Medical Image Analysis*, 12(1):26–41, 2008. Special Issue on The Third International Workshop on Biomedical Image Registration – WBIR 2006. [1, 2, 6, 7](#)
- [5] Fischl B. Freesurfer. *Neuroimage*, 2012. <https://surfer.nmr.mgh.harvard.edu/>. [5](#)
- [6] Ruzena Bajcsy and Stane Kovačić. Multiresolution elastic matching. *Computer Vision, Graphics, and Image Processing*, 46(1):1–21, 1989. [1, 2](#)
- [7] Guha Balakrishnan, Amy Zhao, Mert R. Sabuncu, John Guttag, and Adrian V. Dalca. VoxelMorph: A learning framework for deformable medical image registration. *IEEE Transactions on Medical Imaging*, 38(8):1788–1800, aug 2019. [1, 2, 3, 6, 7, 8](#)
- [8] Ceritoglu C, Wang L, Selemont LD, Csernansky JG, Miller MI, and Ratnanather JT. Large deformation diffeomorphic metric mapping registration of reconstructed 3d histological section images and in vivo mr images. *Front Hum Neurosci*, 2010. [2, 3](#)
- [9] Nicolas Carion, Francisco Massa, Gabriel Synnaeve, Nicolas Usunier, Alexander Kirillov, and Sergey Zagoruyko. End-to-End Object Detection with Transformers. *arXiv e-prints*, page arXiv:2005.12872, May 2020. [3](#)
- [10] UK Centre for Medical Image Computing, University College London. Niftyreg, 2023. <http://cmictig.cs.ucl.ac.uk/wiki/index.php/NiftyReg>. [6, 7](#)
- [11] Junyu Chen, Eric C. Frey, Yufan He, William P. Segars, Ye Li, and Yong Du. TransMorph: Transformer for unsupervised medical image registration. *Medical Image Analysis*, 82:102615, nov 2022. [1, 2, 3, 5, 7, 8](#)
- [12] Junyu Chen, Yufan He, Eric C. Frey, Ye Li, and Yong Du. Vit-v-net: Vision transformer for unsupervised volumetric medical image registration, 2021. [1, 2, 3, 6, 7](#)
- [13] Adrian V. Dalca, Guha Balakrishnan, John Guttag, and Mert R. Sabuncu. Unsupervised Learning for Fast Probabilistic Diffeomorphic Registration. *arXiv e-prints*, page arXiv:1805.04605, May 2018. [2](#)
- [14] Bob D. de Vos, Floris F. Berendsen, Max A. Viergever, Hesam Sokooti, Marius Staring, and Ivana Išgum. A deep learning framework for unsupervised affine and deformable image registration. *Medical Image Analysis*, 52:128–143, feb 2019. [3](#)
- [15] Alexey Dosovitskiy, Lucas Beyer, Alexander Kolesnikov, Dirk Weissenborn, Xiaohua Zhai, Thomas Unterthiner, Mostafa Dehghani, Matthias Minderer, Georg Heigold, Sylvain Gelly, Jakob Uszkoreit, and Neil Houlsby. An image is worth 16x16 words: Transformers for image recognition at scale, 2021. [2, 3, 6](#)
- [16] Beg M. Faisal, Miller Michael I, Trouvé Alain, and Younes Laurent. Computing large deformation metric mappings via geodesic flows of diffeomorphisms. *International Journal of Computer Vision*, 2005. [2](#)
- [17] Ben Glocker, Nikos Komodakis, Georgios Tziritas, Nasser Navab, and Nikos Paragios. Dense image registration through mrfs and efficient linear programming. *Medical Image Analysis*, 12(6):731–741, 2008. Special issue on information processing in medical imaging 2007. [2](#)
- [18] Jing Hu, Ziwei Luo, Xin Wang, Shanhui Sun, Youbing Yin, Kunlin Cao, Qi Song, Siwei Lyu, and Xi Wu. End-to-end multimodal image registration via reinforcement learning. *Medical Image Analysis*, 68:101878, 2021. [2](#)
- [19] Phillip Isola, Jun-Yan Zhu, Tinghui Zhou, and Alexei A. Efros. Image-to-image translation with conditional adversarial networks, 2018. [3, 6](#)
- [20] Max Jaderberg, Karen Simonyan, Andrew Zisserman, and Koray Kavukcuoglu. Spatial transformer networks, 2016. [3, 4](#)
- [21] Diederik P. Kingma and Jimmy Ba. Adam: A method for stochastic optimization, 2017. [4](#)
- [22] Ze Liu, Yutong Lin, Yue Cao, Han Hu, Yixuan Wei, Zheng Zhang, Stephen Lin, and Baining Guo. Swin transformer: Hierarchical vision transformer using shifted windows, 2021. [3, 7](#)
- [23] Dirk Loeckx, Frederik Maes, Dirk Vandermeulen, and Paul Suetens. Nonrigid image registration using free-form deformations with a local rigidity constraint. In Christian Barillot, David R. Haynor, and Pierre Hellier, editors, *Medical Image Computing and Computer-Assisted Intervention – MICCAI 2004*, pages 639–646, Berlin, Heidelberg, 2004. Springer Berlin Heidelberg. [2](#)
- [24] Imperial Collage London. Information extraction from images, 2023. <https://brain-development.org/ixi-dataset/>. [1, 2, 5, 6, 7, 8](#)
- [25] Daniel S. Marcus, Tracy H. Wang, Jamie Parker, John G. Csernansky, John C. Morris, and Randy L. Buckner. Open Access Series of Imaging Studies (OASIS): Cross-sectional MRI Data in Young, Middle Aged, Nondemented, and Demented Older Adults. *Journal of Cognitive Neuroscience*, 19(9):1498–1507, 09 2007. [5, 7](#)

[26] Tony C. W. Mok and Albert C. S. Chung. Large deformation diffeomorphic image registration with laplacian pyramid networks, 2020. 2, 4

[27] Tony C. W. Mok and Albert C. S. Chung. Fast symmetric diffeomorphic image registration with convolutional neural networks, 2021. 2

[28] Tony C. W. Mok and Albert C. S. Chung. Affine medical image registration with coarse-to-fine vision transformer, 2022. 2

[29] Marc-Michel Rohé, Manasi Datar, Tobias Heimann, Maxime Sermesant, and Xavier Pennec. Svf-net: Learning deformable image registration using shape matching. In Maxime Descoteaux, Lena Maier-Hein, Alfred Franz, Pierre Jannin, D. Louis Collins, and Simon Duchesne, editors, *Medical Image Computing and Computer Assisted Intervention - MICCAI 2017*, pages 266–274, Cham, 2017. Springer International Publishing. 2

[30] Ameneh Sheikhhafari, Michelle L. Noga, K. Punithakumar, and Nilanjan Ray. Unsupervised deformable image registration with fully connected generative neural network, 2018. 2

[31] Dinggang Shen and C. Davatzikos. Hammer: hierarchical attribute matching mechanism for elastic registration. *IEEE Transactions on Medical Imaging*, 21(11):1421–1439, 2002. 1, 2

[32] Zhengyang Shen, Xu Han, Zhenlin Xu, and Marc Niethammer. Networks for Joint Affine and Non-parametric Image Registration. *arXiv e-prints*, page arXiv:1903.08811, Mar. 2019. 2, 3

[33] Zhengyang Shen, François-Xavier Vialard, and Marc Niethammer. Region-specific Diffeomorphic Metric Mapping. *arXiv e-prints*, page arXiv:1906.00139, May 2019. 2

[34] Jiacheng Shi, Yuting He, Youyong Kong, Jean-Louis Coatrieu, Huazhong Shu, Guanyu Yang, and Shuo Li. XMorpher: Full Transformer for Deformable Medical Image Registration via Cross Attention. *arXiv e-prints*, page arXiv:2206.07349, June 2022. 2

[35] Hessam Sokooti, Bob de Vos, Floris Berendsen, Boudeijn P. F. Lelieveldt, Ivana Išgum, and Marius Staring. Nonrigid image registration using multi-scale 3d convolutional neural networks. In Maxime Descoteaux, Lena Maier-Hein, Alfred Franz, Pierre Jannin, D. Louis Collins, and Simon Duchesne, editors, *Medical Image Computing and Computer Assisted Intervention - MICCAI 2017*, pages 232–239, Cham, 2017. Springer International Publishing. 2, 3

[36] Robin Strudel, Ricardo Garcia, Ivan Laptev, and Cordelia Schmid. Segmenter: Transformer for Semantic Segmentation. *arXiv e-prints*, page arXiv:2105.05633, May 2021. 3

[37] J.-P. Thirion. Image matching as a diffusion process: an analogy with maxwell’s demons. *Medical Image Analysis*, 2(3):243–260, 1998. 2

[38] Laboratory of Neuro Imaging University of Southern California. Loni probabilistic brain atlas (lpba40), 2023. <https://loni.usc.edu/research/atlas>. 1, 5, 7, 8

[39] Xiao Yang, Roland Kwitt, Martin Styner, and Marc Niethammer. Quicksilver: Fast predictive image registration - a deep learning approach, 2017. 2, 3

[40] Yungeng Zhang, Yuru Pei, and Hongbin Zha. Learning dual transformer network for diffeomorphic registration. In Marleen de Bruijne, Philippe C. Cattin, Stéphane Cotin, Nicolas Padov, Stefanie Speidel, Yefeng Zheng, and Caroline Essert, editors, *Medical Image Computing and Computer Assisted Intervention – MICCAI 2021*, pages 129–138, Cham, 2021. Springer International Publishing. 3

[41] Shengyu Zhao, Yue Dong, Eric Chang, and Yan Xu. Recursive cascaded networks for unsupervised medical image registration. In *2019 IEEE/CVF International Conference on Computer Vision (ICCV)*. IEEE, oct 2019. 4, 8